Review Article

Martin Laurenzis* and Frank Christnacher

Laser gated viewing at ISL for vision through smoke, active polarimetry, and 3D imaging in NIR and SWIR wavelength bands

Abstract: In this article, we want to give a review on the application of laser gated viewing for the improvement of vision cross-diffusing obstacles (smoke, turbid medium, ...), the capturing of 3D scene information, or the study of material properties by polarimetric analysis at near-infrared (NIR) and shortwave-infrared (SWIR) wavelengths. Laser gated viewing has been studied since the 1960s as an active night vision method. Owing to enormous improvements in the development of compact and highly efficient laser sources and in the development of modern sensor technologies, the maturity of demonstrator systems rose during the past decades. Further, it was demonstrated that laser gated viewing has versatile sensing capabilities with application for long-range observation under certain degraded weather conditions, vision through obstacles and fog, active polarimetry, and 3D imaging.

Keywords: 3D imaging; active polarimetry; laser gated viewing; laser speckle reduction; range gating; vision through obstacles.

OCIS code: 110.0110

***Corresponding author: Martin Laurenzis,** French-German Research Institute of Saint-Louis (ISL), 5 Rue du General Cassagnou, 68301 Saint-Louis, France, e-mail: martin.laurenzis@isl.eu
Frank Christnacher: French-German Research Institute of Saint-Louis (ISL), 5 Rue du General Cassagnou, 68301 Saint-Louis, France

1 Introduction

Laser gated viewing has been studied since the 1960s [1] for night vision with long range and through bad weather conditions [1–3]. This method is a promising optronic sensor technology, which is complementary to recent night vision technologies like thermal imaging and intensified low light-level image sensors [4–7]. Owing to enormous improvements in the development of compact and highly efficient laser sources and in the development of modern sensor technologies, the maturity of laser gated viewing systems rose during the past decades, and for instance, commercial systems are available from Obzerv [8], Intevac [9], Selex [10], and Elbit [11]. Main interests in laser gated viewing can be found in target identification and target detection [12–20]. Further, high-performance active imaging systems as well as scientific studies were presented in the field of submarine vision [21–23], vision in scattering environments [24–26], and automotive applications [27, 28]. Further investigations deal with active polarimetry [29–33] as well as 3D imaging [34–42].

In the scope of this publication, the authors want to concentrate on the results of the French-German Research Institute of Saint-Louis (ISL) in the field of laser gated viewing for the improvement of vision cross-diffusing obstacles (smoke, turbid medium, ...), the capturing of 3D scene information, or the study of material properties by polarimetric analysis.

2 Principle of laser gated viewing

In principle, laser gated viewing is the combination and synchronization of a highly sensitive imaging sensor with its own pulsed laser source. This laser source is used to illuminate a scene at the time of observation. Usually, the divergence of the light source is matched to the field-of-view of the imaging device. As illustrated in Figure 1, the scene is illuminated by short laser pulses in the order of a few nanoseconds to microseconds. These laser pulses correspond to a wave train of a few to some hundred meters. Therefore, only a small range of the observed area is illuminated at the same time.

As illustrated in Figure 1, the laser pulse illuminates a scene and is reflected or absorbed by surfaces within the scene. A portion of the reflected light will be reflected

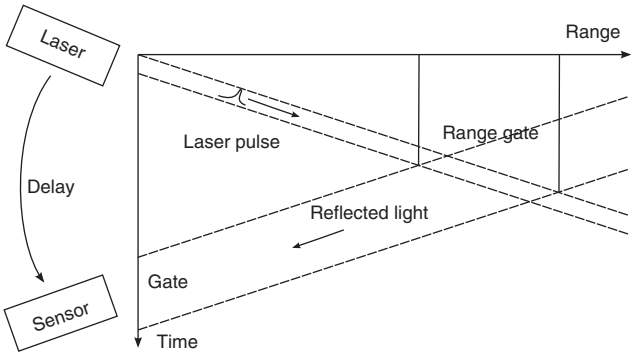

Figure 1 Principle of laser gated viewing.

toward the imaging sensor and carry information about the nature of the scene (like range, reflectivity, and polarization). Owing to the photon time-of-flight, the photons (reflected at different ranges) arrive at different times. While the photons travel toward the scene and back to the sensor, the gate is closed. The sensor is not dazzled by backscattering photons or parasite light sources. The sensor gate opens after a certain time delay for a short integration time. Thus, only light that arrives at the sensor within the right timing window contributes to the imaging process. The range gate is the convolution of the laser pulse and the sensor gate functions. The sensor gate delay determines the position of the range gate in the scene. Therefore, laser gated viewing images contain reflectivity as well as range information.

The differences between laser gated viewing and passive imaging are depicted in Figure 2. Here, a scene at a distance of about 1 km was observed by a passive color TV camera and an active laser gated viewing system. Owing to the illumination by sun light, shadows, and surface reflection can be observed in the passive image (Figure 2A). The spectral information is represented in the color of the pixel. Using laser gated viewing (Figure 2B–D), only the reflection of the applied laser light contributes to the imaging process, and the spectral information is reduced to the laser wavelength (here, λ=1.574 μm). But due to the low parallax between illumination and imaging device, nearly no shadow occurs in the images. For instance, it is possible to look inside shadow areas and inside buildings. A long sensor integration time enables a global view on the scene with a large range gate (see Figure 2B). With a short sensor integration time, only information from a small range gate is recorded. As depicted in Figure 2C, D, it is possible to separate objects from the background and enhance their optical contrast. For example, the object-to-background contrast of the flag is significantly higher in Figure 2C than in Figure 2B. By changing the sensor gate delay, it is possible to place the range gate at different distances.

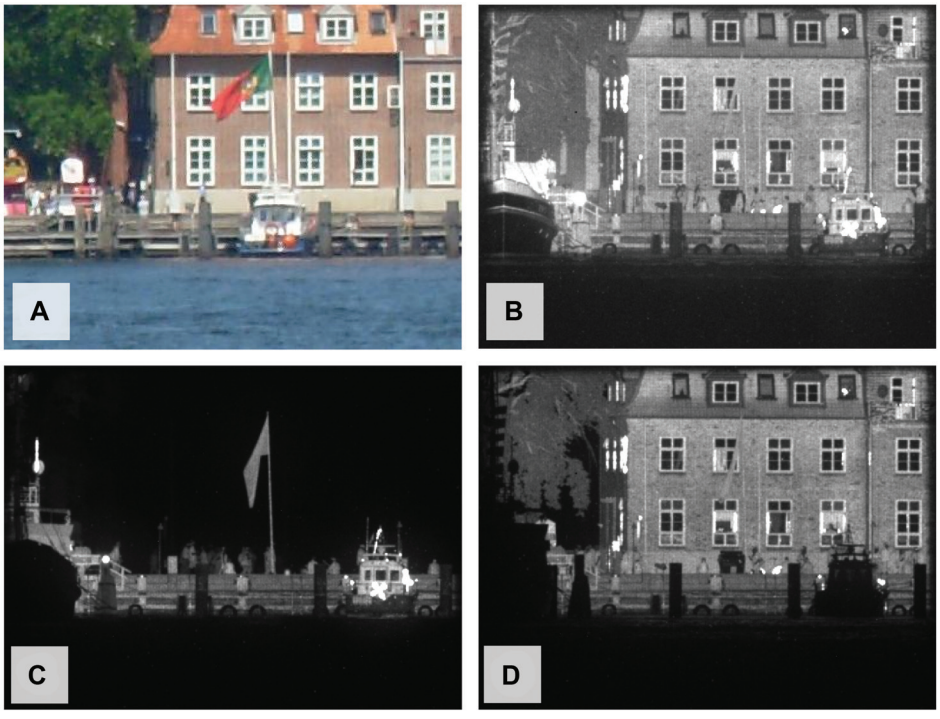

Figure 2 Imaging a scene using (A) passive imaging and laser gated viewing with (B) long integration time and (C, D) short integration with different sensor gate delays.

3 Laser gated viewing at different wavelengths

In the past, laser gated viewing was demonstrated for different laser wavelengths ranging from ultraviolet (UV, solar blind) over visible (VIS), and near-infrared (NIR) to shortwave-infrared (SWIR) wavelengths. Depending on the application and the availability of laser sources and imaging sensors, the use of different wavelengths is recommended. The performance, like the maximum detection range, of these active imaging devices depends on the performances of their components. For instance, the maximum observation range can be estimated from the optical power received by the sensor P_R as calculated by *Paul F. McManamom* [5] [see equation (1)] and the sensor threshold $P_{threshold}$. This threshold value represents a minimal irradiance of the sensor similar to the noise-equivalent photon (NEPh). In the equation, R is the range, and P_T is the transmitted optical power. The target cross-section σ is a factor of the target reflectance and the area of pixel at the target location. Further, A_{illum} and A_{rec} are the areas of illuminated surface and the aperture of the receiver, respectively. The transmission efficiency of the atmosphere and the optical system is described by $\eta_{atm}^2 * \eta_{sys}$. Here, η_{atm}^2 is defined by the Beer-Lambert law as an exponential decay due to atmospheric attenuation by scattering and absorption.

$$P_R = P_T * \frac{\sigma}{A_{illum}} * \frac{A_{rec}}{\pi R^2} * \eta_{atm}^2 * \eta_{sys} \geq P_{threshold} \quad (1)$$

It is evident that the characteristics of the propagation medium have enormous impact on the maximal observation range. Under clear conditions, the maximum range is limited by the decay of irradiance in the scene due to the lateral broadening of the illumination ($\approx R^2$). On the other hand, in very turbid media, the range of a laser gated viewing system is limited by attenuation of light due to absorption and scattering in molecules and particles ($\eta_{atm}^2 = e^{-2\alpha(\lambda)R}$). This physical property is described by the overall attenuation coefficient $\alpha(\lambda) = \alpha_{\text{scattering}}(\lambda) + \alpha_{\text{absorption}}(\lambda)$.

3.1 Laser gated viewing at NIR wavelengths

In the NIR wavelength band, laser gated viewing systems become more and more mature. The NIR band covers a wavelength range from 780 nm to 900 nm. Owing to the availability of high-power laser diodes, mainly wavelengths of 808 nm–860 nm lengths are used. On the sensor side, high-performing light intensifiers can be coupled to high-resolution and commercially available imaging sensors and cameras. These components allow the development of compact, lightweight, and power-efficient systems.

For instance, in Figure 3, two ISL demonstrator systems are depicted. The prototype on the left hand is a long-range laser gated viewing system having a field-of-view of 1°×0.8°. It allows the observation of objects at a range of more than 12 km and is particularly suitable for surveillance missions and long-range identification.

Figure 3 Compact demonstrators of ISL for laser gated viewing based on laser diode illumination at NIR wavelength.

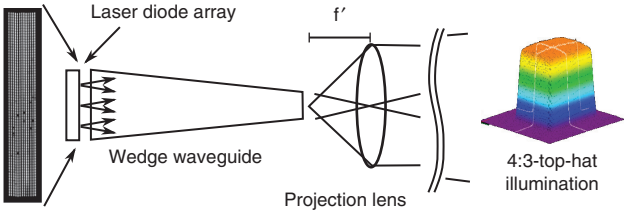

Figure 4 Beam shaping of a laser diode stack by a wedge waveguide for homogeneous top-hat illumination profiles (ISL patented [28, 29]).

The right-hand system has a medium operation range of about 3 km and a switchable field-of-view from 6.1°×4.6° to 2.6°×1.6°. The illumination devices are based on laser diode arrays emitting laser pulses at 808 nm with variable pulse widths and peak powers up to some kilowatts. Both demonstrators are able to accumulate over several laser pulses by multiple exposures. Typically, the imaging sensor integrates a few hundred laser pulses for a single image.

The radiation emitted by laser diodes is highly divergent with different divergence angles for the fast and the slow axis and a high M^2 value. The challenge in the application of laser diode stacks for illumination issues is the collimation and beam shaping of the laser to realize a homogeneous illumination of the scene. Without a proper collimation technique, inhomogeneous illumination occurs, and the performance of the laser gated viewing system is reduced. At ISL, a waveguide-based collimation technique was developed [43, 44] to enable a homogeneous rectangular illumination [33]. As depicted in Figure 4, the waveguide is used for homogenization by multiple internal reflections and for the reduction of the emitting surface to match the dimension of the imaging sensor. A perfect matching of the laser illumination field and the sensor field-of-view enables an efficient use of the sensor array and laser power. For the application of NIR laser illumination devices, the laser safety restrictions have to be taken into account. For security reasons, a laser safety distance, i.e., the non-ocular hazardous distance (NOHD), has to be calculated from the laser safety regulations [45] to avoid surpassing the maximum permissible exposure (MPE).

In Figure 5, two examples for the application of laser gated viewing at NIR wavelengths (λ=808 nm) are presented. In image A, the long-range prototype was used for surveillance and reconnaissance in maritime environment, i.e., the detection and classification of surface vessels in a range of 4 km–12 km. In image B, the medium range system was applied to demonstrate the observation of persons inside a vehicle at a distance of 300 m.

3.2 Eye-safe laser gated viewing at SWIR wavelength

Owing to the capability of laser gated viewing to enable vision through scattering media, like fog and smoke, more and more interests rise for civilian and security applications. In this context, the issue of eye safety is inevitably for debate to work in the so-called eye-safe wavelength band at around 1.4 µm–2.2 µm, i.e., the shortwave infrared (SWIR). Within this spectral range, water has a high absorption coefficient. For instance, laser radiation is absorbed on an eye's surface before it is focused on the retina. Thus, the maximum permissible exposure (MPE) is significantly higher than in the visible spectral range [45]. Further, compared to higher infrared bands (MWIR and LWIR), the thermal emission is low. Therefore, no parasite light from thermal emission can be observed at ambient temperature in this wavelength band.

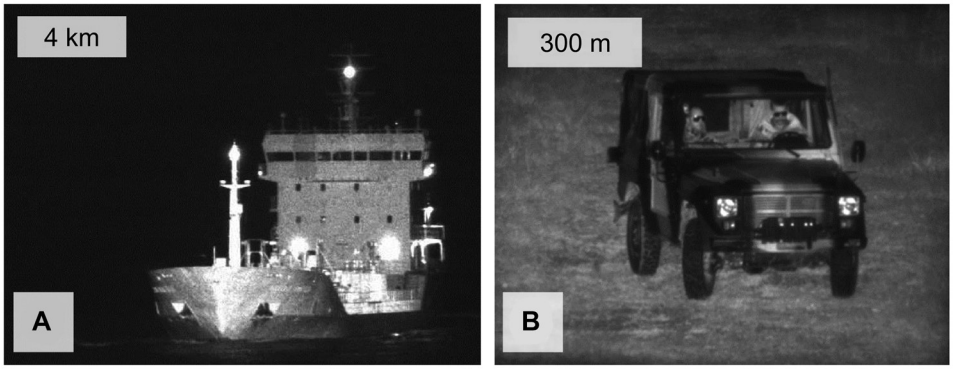

Figure 5 Examples for laser gated viewing at 808 nm at different scenarios: (A) Monitoring maritime traffic and (B) vision through a window of a vehicle.

Figure 6 Image of the ISL eye-safe active imaging system.

In the SWIR wavelength band, the number of different sensor devices, which have sufficient performances by means of high sensitivity and the ability of gating is limited to a few electron-bombarded and electron-multiplying sensor devices. Until now, only an exposure of the imaging sensor with a single laser pulse illumination is possible. Therefore, the illumination device has to use a high-energy pulse illumination, which is only provided by solid state laser sources. In Figure 6, an ISL demonstrator is shown, using an EBCMOS imaging sensor and a Nd:YAG KTP OPO solid state laser illumination device. The laser source has a pulse power of 65 mJ at 1.574 µm with a repetition rate of 25 Hz. This laser source has to be water cooled. The depicted laser gated viewing system has a field-of-view of 1.5°×1° and an operation range of about 3 km.

Compared to the application of laser diodes, the application of a solid state laser source for illumination issues challenges different problems. Owing to low divergence and a small M^2 value, the effort of beam shaping is lower, but the high coherence of solid state laser leads to laser speckle, which reduces the imaging quality of a laser gated viewing system. In the literature, different approaches have been demonstrated using temporal [13], spectral [36, 46], and spatial [33] diversity to reduce the laser speckle. At ISL, an illumination with spatial diversity was realized using a waveguide for collimation and beam shaping of the solid state laser source, as depicted in Figure 7. Here, the laser beam is coupled into a bar-type waveguide, and the homogeneous intensity distribution of the exit facet is projected to the illuminated scene. In front of the projection lens, a plane of virtual sources is generated by imaging of multiple reflections of the focus point. These virtual sources cause spatial diversity within the illumination process.

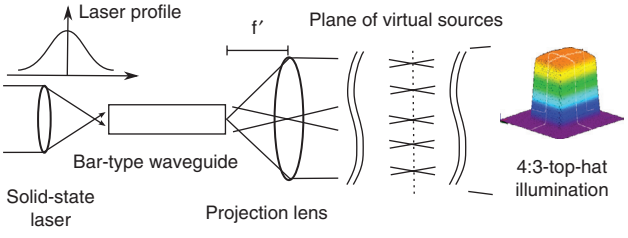

Figure 7 Beam shaping of solid state laser by bar-type waveguide for homogeneous illumination and reduction of laser speckle effects (ISL patented [28, 29]).

In Figure 8, the laser speckle reduction capability of the ISL illumination approach is demonstrated. Figure 8A shows an illumination from a single laser source. The high amount of laser speckle leads to significant loss of optical resolution of details in the image. Using the ISL approach (Figure 8B), the superposition of the illumination from different virtual sources reduces the amount of laser speckle. More details can be resolved by the imaging sensor. Both images were recorded with the same active imaging system and with single laser pulse illumination.

4 Application of laser gated viewing

As aforementioned, laser gated viewing has different applications in the field of target detection and identification as well as vision through obstacles, active polarimetric and 3D imaging.

4.1 Vision through smoke

In passive imaging, the vision through fog and smoke is limited by attenuation (absorption and scattering) of light

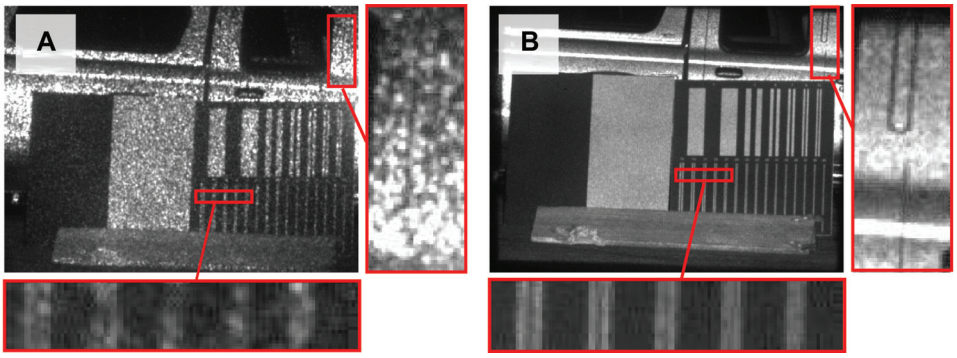

Figure 8 Laser gated viewing based on solid state laser illumination (A) without waveguide and (B) with waveguide.

from the scene and by dazzling of the imaging sensor by scattered light from external light sources (e.g., sunlight). In contrast, laser gated viewing is capable to penetrate scattering media (fog, smoke, water, etc.) as long as a small amount of photons can pass through these obstacles without scattering. Ballistic photons, i.e., the undisturbed information, arrive at different times at the sensor than backscattered photons. Therefore, by means of gated viewing, it is possible to temporally filter the information and separate ballistic photons. Further, due to very short integration times, no dazzling of the imaging sensor occur from scattered external or parasite light sources. For instance, in Figure 9, the imaging of a scene containing smoke with a color camera (A) and a SWIR laser gated viewing system (B) is compared. While the color camera is dazzled by scattered sunlight (integration time 20 ms), the SWIR system is capable of penetrating the smoke and enable a clear and undisturbed vision of the scene (integration time 500 ns).

4.2 Active polarimetric imaging

The interaction of light with object surfaces is described in the Stokes-Muller formalism, as defined in equation (2). Here, M is the 4×4 Muller matrix, which characterizes the interaction of light with the object surface, and S is the four-element stokes vector, which describes the properties of the light.

$$\vec{S}_{detected} = M \cdot \vec{S}_{emitted} \tag{2}$$

Polarimetric imaging is used to analyze the polarization of reflected light to reveal the nature of surfaces. Owing to the nature of different surfaces, they have different impact on the polarization state of light. Therefore, active polarimetric imaging is a widely used method in remote sensing [29–33].

Typically, the illumination device of a laser gated viewing system uses light with a strong polarization. Even the homogenization and collimation do not harm the polarization of the illumination beam. Therefore, the polarization state of the reflected light can be analyzed to realize active polarimetric imaging. For instance, in Figure 10, an example of active polarimetric imaging at 808 nm and at a distance of 300 m is presented. Here, the overall intensity (A) is compared with the orthogonal state contrast (OSC) for linear (B) and circular (C) polarized illumination. This measure is defined as $OSC = \frac{(I_{\parallel} - I_{\perp})}{(I_{\parallel} + I_{\perp})}$

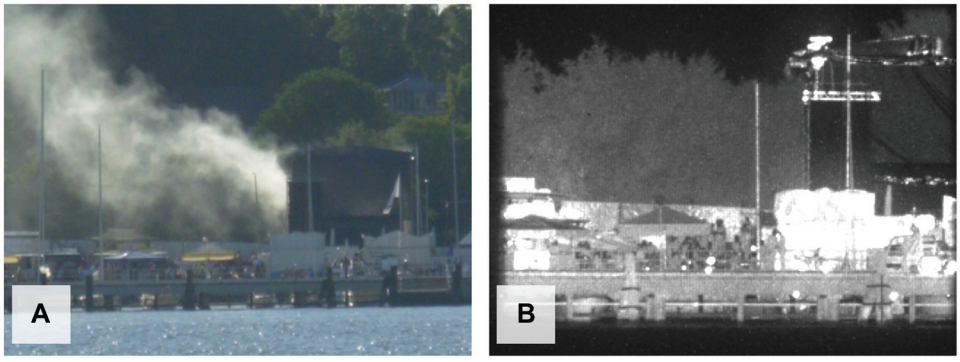

Figure 9 Vision through a smoke: (A) passive imaging and (B) laser gated viewing.

Figure 10 Intensity (A) and orthogonal state contrast for illumination with linear (B) and circular (C) polarized laser.

and can be calculated for each pixel from two images with perpendicular polarization. The linear and circular OSC represent the diagonal elements M_{22} (and M_{33}) and M_{44} of the Muller matrix, respectively. The OSC can be used to distinguish artificial objects from vegetation.

4.3 3D imaging

A further application of laser gated viewing is 3D imaging. As depicted in Figure 11, two different methods have reached high maturity and were discussed in the literature.

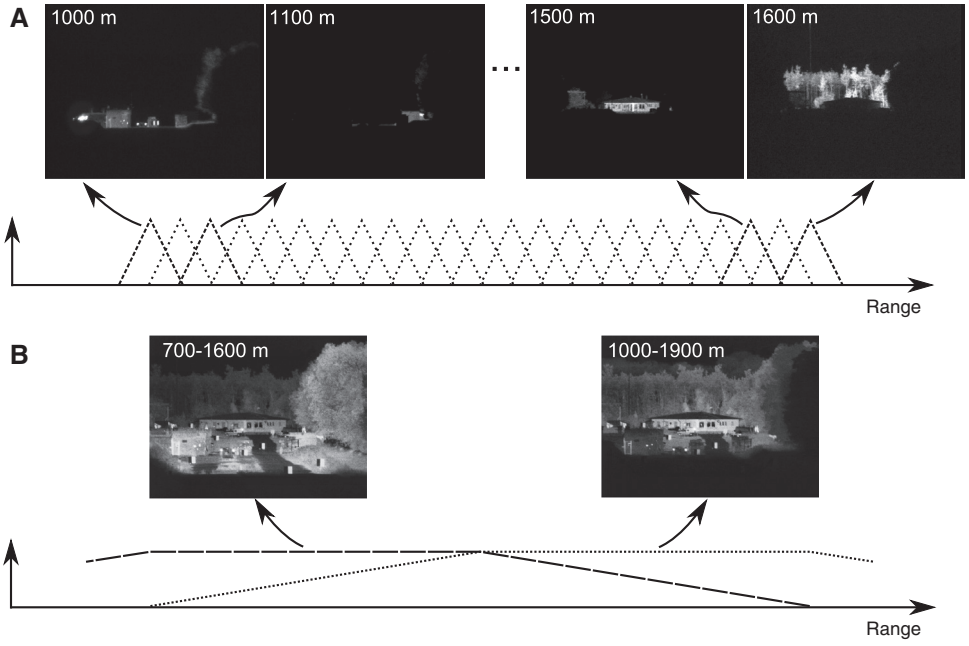

Figure 11 Sampling range information for 3D imaging by laser gated viewing with (A) a sliding range gate and (B) overlapping range gates.

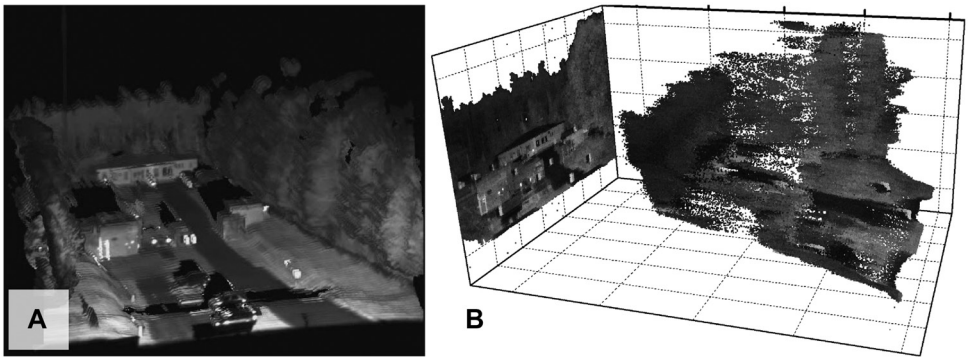

Figure 12 Two 3D display methods of depth information: (A) 3D model and (B) point cloud.

In the sliding gate or tomography method [34–38], the variation of the sensor delay is used to sample a scene with a small range gate (Figure 11A). Owing to the Nyquist sampling theorem, smaller range gates and finer sensor-delay steps lead to higher depth resolution. Depending on the sampling range and the sought accuracy [i.e., signal-to-noise ratio (SNR), depth resolution ...] a more or less huge amount of frames has to be recorded and analyzed for the calculation of depth information. For instance, a single target, like a car or van, can be a sample with sufficient SNR and depth resolution in 10–100 frames [34–38], while the sampling of a more complex scenario, like a 3D environment model, can exceed more than a thousand frames.

An alternative approach to calculate depth information from a few recorded images is the depth-profile analysis or intensity correlation method [38–42]. As depicted in Figure 11B, this method is based on the analysis of gray level changes of overlapping range gates. Only the gray level information of two images is needed, where in one image the scene is fully illuminated, and in the other image, the same region is only partly illuminated by the edge of the range gate. Then, the dynamic range of the range gate is use to calculate the depth of the scene. Despite the fact that the accuracy of this method depends on the signal height, it is able to overcome the Nyquist sampling theorem and perform super-resolution depth mapping [39].

Owing to the fact that the total number of frames required for scene reconstruction can be kept low enough, acquisition times become reasonable using the performance of current lasers and sensor technology, even at quite long ranges. This makes 3D imaging from laser gated viewing work in practice. The calculated depth information can be used for 3D reconstruction, 3D display, and 3D analysis (e.g., point-to-point measurement). For instance, in Figure 12, two methods of 3D display are presented. In Figure 12A, a 3D model of a scenario is shown. Here, the observation point is virtually changed to an upper-left position. In Figure 12B, the 3D data is depicted as a point cloud.

5 Conclusions

Laser gated viewing has been studied since the 1960s as an active night vision method. Owing to enormous improvements in the development of compact and highly efficient laser sources and in the development of modern sensor technologies, the maturity of demonstrator systems rose during the past decades. Further, it was demonstrated that laser gated viewing has versatile sensing capabilities with application for long-range observation under all-weather condition, vision through obstacles and fog, active polarimetry, and 3D imaging. Thus, laser gated viewing is a promising sensor technology, which is complementary to recent night vision technologies like thermal imaging and intensified low light-level image sensors.

Received July 12, 2013; accepted August 29, 2013; previously published online October 2, 2013

References

[1] L. F. Gillespie, JOSA 56, 883–887 (1966).
[2] H. Steingold and R.E. Strauch, Appl. Opt. 8, 147–154 (1969).
[3] C. W. Lamberts, Appl. Opt. 15, 1284–1289 (1976).
[4] I. Baker, D. Owton, K. Trundle, P. Thorne, K. Storie, et al., Proc. SPIE 6940, 6902L (2008).
[5] P. F. McManamon, Opt. Eng. 51, 060901 (2012).

[6] O. David, R. Schneider and R. Israeli, Proc. SPIE 7482, 748203 (2009).
[7] O. Steinvall, M. Elmqvist, T. Chevalier and O. Gustafsson, Appl. Opt. 52, 4763–4778 (2013).
[8] Obzerv Inc., 400 Jean-Lesage, Québec Qc, Canada, http://www.obzerv.com/.
[9] Intevac, Inc., 3560 Bassett Street, Santa Clara, CA 95054, USA, http://www.intevac.com/.
[10] Selex ES Ltd., Christopher Martin Road, Basildon, Essex, SS14 3EL, UK, http://www.selex-es.com/.
[11] Elbit Systems Ltd., P.O.B 539, Haifa 31053, Israel, http://www.elbitsystems.com/.
[12] O. Steinvall, H. Olsson, G. Bolander, C. Carlsson and D. Letalick, Proc. SPIE 3707, 432–448 (1999).
[13] R. G. Driggers, R. H. Vollmerhausen, N. Devitt, C. Halford and K. J. Barnard, Opt. Eng. 42, 738–746 (2003).
[14] O. Steinvall, H. Larsson, F. Gustafsson, T. Chevalier, A. Persson, et al., Proc. SPIE 5613, 51–66 (2004).
[15] R. L. Espinola, E. L. Jacobs, C. E. Halford, R. Vollmerhausen and D. H. Tofsted, Opt. Exp. 15, 3816–3832 (2007).
[16] D. Bonnier, S. Lelievre and L. Demers, Proc. SPIE 6206, 62060A (2006).
[17] D. Dayton, S. Browne, J. Gonglewski, S. Sandven, J. Gallegos, et al., Opt. Eng. 40, 1001–1009 (2001).
[18] O. Steinvall, M. Elmqvist and H. Larsson, Proc. SPIE 8186, 818605 (2011).
[19] O. Steinvall, T. Chevalier, P. Andersson and M. Elmqvist, Proc. SPIE 6542, 654218 (2007).
[20] O. Steinvall, P. Andersson, M. Elmqvist and M. Tulldahl, Proc. SPIE 6542, 654216 (2007).
[21] G. R. Fournier, D. Bonnier, J. L. Forand and P. Pace, Opt. Eng. 32, 2185–2190 (1993).
[22] E. A. McLean, H. R. Burris, Jr. and M. P. Strand, Appl. Opt. 34, 4343–4351 (1995).
[23] J. Busck, Opt. Eng. 44, 116001 (2005).
[24] M. Laurenzis, F. Christnacher, E. Bacher, N. Metzger, S. Schertzer, et al., Proc. SPIE 8186, 818603 (2011).
[25] M. Laurenzis, F. Christnacher, D. Monnin and T. Scholz, Opt. Eng. 51, 061303 (2012).
[26] E. Belin, F. Christnecher, F. Taillade and M. Laurenzis, Proc. SPIE 7088, 70880O (2008).
[27] O. David, N. S. Kopeika and B. Weizer, Appl. Opt. 45, 7248–7254 (2006).
[28] F. Christnacher, J.-M. Poyet, M. Laurenzis, J.-P. Moeglin and F. Taillade, Proc. SPIE 7675, 76750J (2010).
[29] S. Breugnot and P. Clemenceau, Opt. Eng. 39, 2681–2688 (2000).
[30] M. A. Miller, R. V. Blumer, and J. D. Howe, Proc. SPIE 4481, 87–99 (2002).
[31] D. A. Lavigne, M. Breton, M. Pichette, V. Larochelle and J. R. Simard, Proc. SPIE 6972, 69720x (2008).
[32] M. Alouini, F. Goudil, A. Grisard, J. Bourderionnet, D. Dolfi, et al., Appl. Opt. 48, 1610–1618 (2009).
[33] M. Laurenzis, Y. Lutz, F. Christnacher, A. Matwyschuk and J. M. Poyet, Opt. Eng. 51, 061302 (2012).
[34] J. Busck and H. Heiselberg, Appl. Opt. 43, 4705–4710 (2004).
[35] P. Andersson, Opt. Eng. 45, 034301 (2006).
[36] E. Repasi, P. Lutzmann, O. Steinvall, M. Elmqvist, B. Göhler et al., Appl. Opt. 48, 5956–5969 (2009).
[37] B. Göhler and P. Lutzmann, Proc. SPIE 8542, 854205 (2012).
[38] D. Monnin, A. L. Schneider, F. Christnacher, and Y. Lutz. 3DPVT, IEEE Computer Society 938–945 (2006).
[39] M. Laurenzis, F. Christnacher and D. Monnin, Opt. Let. 32, 3146–3148 (2007).
[40] X. Zhang and H. Yan, Appl. Opt. 50, 1682–1686 (2011).
[41] M. Laurenzis and E. Bacher, Appl. Opt. 50, 3824–3828 (2011).
[42] M. Laurenzis, E. Bacher, S. Schertzer and F. Christnacher, Proc. SPIE 8186, 818604 (2011).
[43] Y. Lutz, "Device for collimating a high-brightness laser diode array" patent: FR2845776/US2004165643/DE10341531.
[44] Y. Lutz, "Illuminateur laser/Uniform illumination apparatus", patent: EP1712940/FR2884621/US2007019912.
[45] "Safety of laser products – part 1: Equipment classification and requirements", European norm: EN 60825-1, CENELEC, Brussels.
[46] B. Göhler, P. Lutzmann, G. Anstett, Proc. SPIE 7113, 711307 (2008).

Martin Laurenzis obtained his MSc in Physics from the University of Dortmund (Germany) and his PhD in Electrical Engineering and Information Technology from the University of Aachen (Germany). He is specialized in the area of night vision systems and active imaging with a particular interest in vision in poor weather conditions. He is currently developing new 3D techniques and new theoretical tools for performance evaluation of 3D active imaging systems.

Frank Christnacher received his MSc and his PhD from the University of Haute-Alsace (France) in the field of Optical Data Processing and Pattern Recognition. He is currently the head of the Optronics and On-Board Visionics group of the French-German Research Institute of Saint-Louis. Specialized in the area of night vision imaging systems and active imaging, he is particularly interested in long-distance vision and in vision in degraded weather conditions. He initiated and led numerous international scientific collaborations.